UNIVERSITY *of* York

This is a repository copy of *Optimising Low Temperature Pyrolysis of Mesoporous Alginate-Derived Starbon® for Selective Heavy Metal Adsorption*.

White Rose Research Online URL for this paper:
https://eprints.whiterose.ac.uk/id/eprint/212161/

Version: Published Version

White Rose
university consortium
Universities of Leeds, Sheffield & York

eprints@whiterose.ac.uk
https://eprints.whiterose.ac.uk/

Optimising Low Temperature Pyrolysis of Mesoporous Alginate-Derived Starbon® for Selective Heavy Metal Adsorption

Nicholas Garland,*[a] Ross Gordon,[b] Con Robert McElroy,[c] Alison Parkin,[a] and Duncan MacQuarrie*[a]

In response to the ever increasing need to develop more efficient and sustainable methods for removing heavy metal contaminants from aqueous systems, the following article reports on the design of highly mesoporous alginate-derived materials (Starbon®) and their application to the adsorption of heavy metals. Using the Starbon® process to expand, dry and pyrolyse an inherently porous polysaccharide precursor, it was possible to produce mesoporous materials (BJH mesopore volumes $0.81–0.94\ cm^3\,g^{-1}$) with large surface areas (157–297 $m^2\,g^{-1}$) across a range of low pyrolysis temperatures (200–300 °C). The mechanisms of thermal decomposition were explored in terms of chemical and structural changes using N_2-sorption porosimetry, thermogravimetric analysis, titration, FT-IR spectroscopy and ^{13}C NMR spectroscopy. It was found that, as a result of intermolecular dehydration and crosslinking, sufficient chemical stability is obtained by the intermediate temperature of 250 °C, with limited improvement seen at higher temperatures. In addition, the materials retained large metal adsorption capacities (0.70–1.72 $mmol\,g^{-1}$) as well as strong selectivity for Cu^{2+} ions (over Co^{2+} and Ni^{2+}), as compared to commercial petrochemical-derived cation exchange resin Amberlite™ Mac 3H. Thus, highlighting the potential of Starbon® materials as a sustainable answer to the widespread problem of heavy metal-contaminated wastewaters.

Introduction

Recent estimates suggest that over 2 billion people worldwide do not have access to clean drinking water.[1] In particular, due to ever increasing industrial development and their persistent toxicity, heavy metal contamination presents an increasing risk from both human and ecological health perspectives.[2–4] As a result, there is a need to develop more efficient and cost effective methods for removing these metals from both industrial effluents and from contaminated drinking water sources. While a range of newer technologies are currently adopted for the removal of heavy metals from water, including reverse osmosis, nanofiltration and ion exchange, metal removal by adsorption remains generally the most cost effective and, for many metal ions, the most efficient option.[5]

With the potential to be produced inexpensively from bioderived feedstocks, porous pyrolytic carbon materials have received considerable attention for their application towards the adsorption of metals from aqueous solutions.[6,7] In addition to being low cost, pyrolytic materials are practically easy to use and tend to have excellent chemical and mechanical stability, enabling their regeneration and reuse over long periods.[8] Often reliant on chemical or thermal activation to impart porosity, unmodified carbon materials provide access to a limited range of surface chemistries.[9,10] As a result, chemical functionalisation is required to provide sufficient capacities for the removal of heavy metal ions.[8,11,12]

Alginic acid is a linear copolymer of 1,4-linked β-D-mannuronic and α-L-guluronic acid residues in varying proportions. Largely sourced from brown algae, the polymer has an enormous natural abundance and presents a very sustainable feedstock for the production of functional materials.[13,14] Upon the exchange of acidic protons for a range of metal cations, alginic acid forms an insoluble gel, the so called 'egg-box structure', whereby alginate polymers become ionically cross-linked via a metal cation coordinated to two neighbouring carboxylate groups (Figure 1).[15,16] To this end, alginate gels have similarly been suggested for their ability to adsorb large quantities of heavy metals.[17]

Alginic acids are known to chelate a wide range of divalent and trivalent metal cations, including Pb^{2+}, Cu^{2+}, Cd^{2+}, Ba^{2+}, Sr^{2+}, Ca^{2+}, Mn^{2+}, Zn^{2+}, Co^{2+}, Ni^{2+} and Fe^{3+}, to name a few. Unsurprisingly, alginate gels have been investigated for their potential application to wastewater remediation many

[a] N. Garland, Prof. A. Parkin, Dr. D. MacQuarrie
Department of Chemistry
University of York
Heslington, York, YO10 5DD (UK)
E-mail: nphg500@york.ac.uk
duncan.macquarrie@york.ac.uk

[b] Dr. R. Gordon
Jonson Matthey Technology Centre
Sonning Common, Reading, RG4 9NH (UK)

[c] Dr. C. R. McElroy
School of Chemistry
University of Lincoln
Lincoln, LN6 7TS (UK)

ChemSusChem

Research Article
doi.org/10.1002/cssc.202400015

Chemistry
Europe
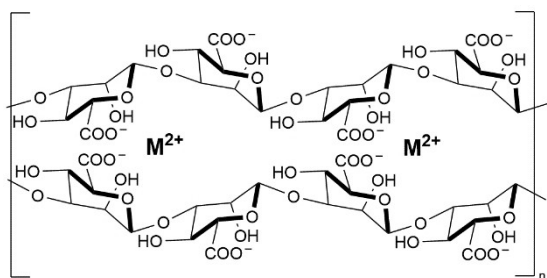European Chemical
Societies Publishing

Figure 1. Proposed structure of metal–alginate chelate gel.

times.[18,19] With large capacities for metal ions (ca. 3 mmol g^{-1}), comparable to those of commercial cation exchange resins, alginate gels appear to be an excellent candidate.[20,21] However, to be applied to real wastewaters the issues of mechanical and chemical stability must first be addressed. As with many polysaccharides, alginic acid will undergo hydrolysis at both excessively high or low pH and it presents more or less complete incompatibility with Na$^+$, which results in the formation of the water-soluble Na–alginate salt.[22,23]

To overcome the issues associated with poor mechanical strength, alginates have been composited with a wide range of materials including activated carbon, graphite, silicas, Fe_3O_4, and TiO_2.[24–29] These composites are seen to improve upon several of the physical properties of alginate gels including mechanical strength, surface area and swelling, all of which are essential for the application of these materials in fixed beds and columns, but do not address the underlying chemical instability issues.

First published in 2006 by Budarin et al., Starbon® materials ("starbons") are a novel group of non-templated carbons that possess predominantly macro and mesoporosity in addition to large surface areas (100–1000 m^2 g^{-1}), comparable to activated carbons.[30,31] Based upon inherently porous polysaccharide gel precursors, due to the patented manufacturing process, Starbons are not reliant on pore activation by pyrolysis. As a result, these materials possess high porosity across a wide range of pyrolysis temperatures and subsequent surface chemistries.[32,33] While similar surface chemistries and porosities may be achieved using inorganic-polysaccharide composites and templated materials, their production is inherently more complex and wasteful, requiring the use of auxiliaries and additional steps.[34,35] Accordingly, Starbons present the potential to be applied on much larger scales at lower costs and in a more sustainable manner. By the application of the Starbon® process to alginic acids at lower pyrolysis temperatures (0–300 °C), we anticipate the potential to produce stable materials that largely retain the metal chelating ability of alginic acid.

The work reported herein aims to explore the chemical and textural changes that occur at low temperatures (0–300 °C) when alginic acid aerogels are pyrolysed using the Starbon® process. While pyrolysis to excess of 300 °C is understood to impart excellent chemical and mechanical stability to Starbon® materials, it is not clear how the material chemistry changes up to this point as relates to metal adsorption applications. In particular, as pyrolysis temperature is increased, we aim to explore the compromise between the anticipated drop in metal adsorption capacity with the increasing degree of crosslinking (and subsequent chemical stability). To this end, a series of four alginate-derived Starbons were produced at a range of pyrolysis temperatures for characterisation, A000, A200, A250 and A300.

Results and Discussion

Production of Alginate Aerogel A000

Using the Starbon® process reported by Borisova et al.,[35] an A000 material was produced from alginic acid via the following steps:
- expansion of alginic acid in water at 90 °C
- addition of t-butanol to the hydrogel to form a eutectic mixture
- removal of t-butanol/water via freeze drying

Resulting in the extensively mesoporous (mesopore volume = 1.55 cm^3 g^{-1}, surface area = 286 m^2 g^{-1}) A000 material that was subsequently pyrolysed under reduced pressure to a range of temperatures to yield the A200, A250 and A300 materials studied herein. While seen to introduce extensive porosity, expansion and removal of solvent does not result in any observed chemical change to the alginic acid precursor, as evidenced by initial characterisation. Analysis of A000 yielded an FTIR spectrum characteristic of alginic acid (*vide infra*) and acidic concentration of 6.2 mmol g^{-1}, determined by titration with NaOH, in close agreement with the predicted 5.7 mmol g^{-1}.[36]

Characterisation of Chemical and Structural Changes that Accompany Low Temperature Pyrolysis of A000

Visual inspection of the materials produced from the low temperature pyrolysis of A000 (Figure S1) reveals significant change from the white solid A000 precursor towards the dark brown/black, characteristic of biochars, at temperatures as low as 200 °C. Contrastingly, electron microscopy of the materials suggests very little change to the macro structure between 0–300 °C. Scanning electron microscopy (Figure 2) reveals the hierarchical fibrous structure of A000 which is expected to arise as a result of the specific conditions under which the alginic acid precursor is gelled.[37] Upon pyrolysis (< 300 °C), the macro structure is not seen to change appreciably with the average particle size and morphology being conserved (Figure S5).

Despite the lack of morphological change, gravimetric analysis (Figure 3) reveals the loss of ~63.5 wt% during the pyrolysis of A000 to 300 °C. Over this range, two distinct mass loss events are identified: the loss of 11.5% between 0–150 °C and the loss of a further 52% between 150–300 °C. Additionally, SEM-EDX elemental analysis (Table S1) reveals a significant change in the relative amounts of C, H and O, with almost no inorganic contribution, indicative of major chemical change occurring over this temperature range. To further characterise
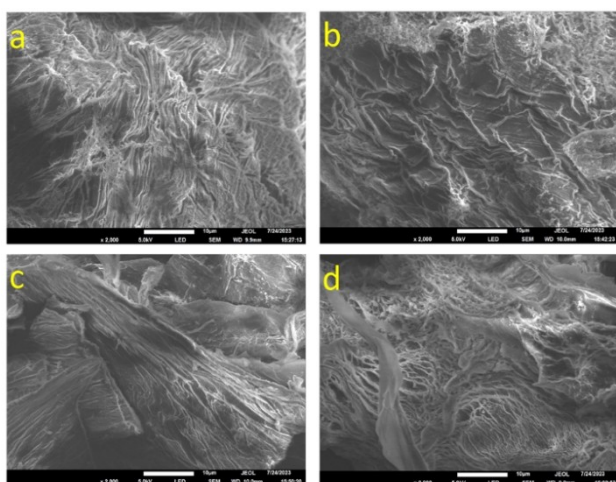
ChemSusChem

Research Article
doi.org/10.1002/cssc.202400015

Chemistry
Europe
European Chemical
Societies Publishing

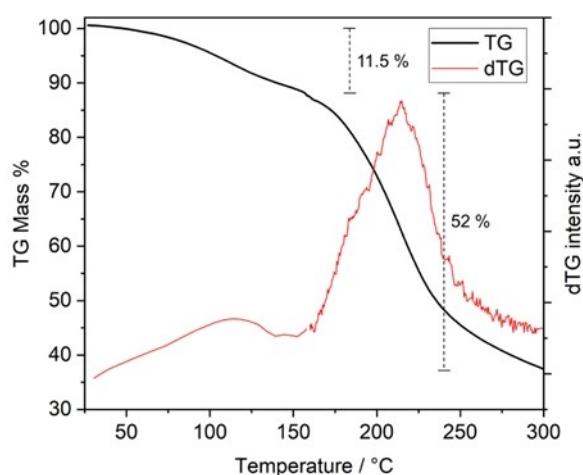**Figure 2.** SEM micrographs of a) A000, b) A200, c) A250 and d) A300.

Figure 3. Thermal gravimetric analysis of A000 heated from 20 to 300 °C under N_2. Left y axis – thermal gravimetric (TG) percentage mass loss (black line); right y axis – first derivative of the TG trace (dTG, red line). Mass loss during individual events indicated by dashed lines.

the changes in chemical functionality and micro/meso structure occurring during low temperature pyrolysis, a range of techniques have been employed.

0–200 °C During the early stages of pyrolysis, initial mass loss (below 150 °C) is attributed to evaporation of physisorbed water. This is consistent with CHN analysis of A000 (Table S2), which indicates the presence of 12 wt% water in addition to the $C_6H_8O_6$ polysaccharide starting material (Figure 4a). According to thermal analysis (Figure 3) beyond 150 °C, a second mass loss event begins. This event is attributed to chemical decomposition. A comparison of the elemental compositions of A000 and A200 (Figure 4a) reveals the loss of a significant amount of H and O from the polysaccharide structure, with very limited loss of C. This change in elemental composition suggests that mass loss below 200 °C is almost exclusively a result of evolution of water, initially, thermal desorption and later due to chemical decomposition.

Transmission FTIR analysis of A000 and A200 in Figure 4b indicates a loss of hydroxyl functionality, characterised by a stretch at 1050 cm^{-1}, during the initial decomposition. A similar decrease in the intensity of the signal attributed to hydroxyl groups is seen in the solid-state ^{13}C MAS NMR at 60–90 ppm (Figure S8). Additionally, ^{13}C NMR reveals a significant increase in the aliphatic carbon content (<60 ppm) upon heating to 200 °C. This dehydration is consistent with existing understanding of the thermal decomposition of polysaccharides and is known to be catalysed by the presence of acidic groups.[31,38] In addition to the substantial mass loss upon pyrolysis to 200 °C, comparison of the N_2-sorption porosimetry of A000 and A200 reveals a significant decrease in the total pore volume (Figure 4c). It has been suggested previously that this contraction of mesopore structure occurs as a result of the intermolecular dehydration and crosslinking evidenced by loss of water and disappearance of hydroxyl functionality from the FTIR.[38]

In good agreement with the elemental analysis in Figure 4a, the concentration of acidic groups (Figure 4d), is seen to be conserved upon pyrolysis to 200 °C.

200–250 °C Upon heating from 200 °C to 250 °C, thermal analysis indicates further loss of 27.3 wt% with the rate of mass loss due to thermal decomposition reaching a maximum at 216 °C. Over this temperature range, elemental analysis reveals further loss of H and O in addition to the first significant loss of C. Consistent with this, FTIR indicates the decomposition of the remaining hydroxyl functionality (1050 cm^{-1}), expected to result from significant dehydration of the polysaccharide structure. In addition to the intermolecular dehydration seen to contribute to the mesopore contraction, intramolecular dehydration is expected to result in increasingly unsaturated structures.[39] This is manifested as a decrease in the vibrational frequency of conjugated carbonyl groups (1700–1800 cm^{-1}), the growth of a signal attributed to unsaturation at ca. 1600 cm^{-1}, and is observed directly in the evolution of species such as furfural at 210–300 °C (Figure S4). ^{13}C NMR (Figure S8) reveals both the loss of remaining hydroxyl groups and the formation of a significant signal at 100–160 ppm attributed to the formation of unsaturation.

In addition to the loss of water, the significant loss of acidity seen in Figure 4d may be attributed to increased decomposition of carboxylate groups at higher temperatures and accounts for the loss of C from the structure. Despite the significant chemical transformation, the very small change in pore volume (Figure 4c) seen between 200–250 °C suggests that the only significant change to the mesoporous structure occurs during the initial dehydration (below 200 °C).

250–300 °C Pyrolysis to 300 °C results in the further loss of just 8.1 wt%, indicative of the decreased rate of chemical change occurring during the final stage of pyrolysis. Additionally, there is no significant change to the elemental composition of A250 upon heating to 300 °C. Comparison of the FTIR of A250 and A300 (Figure 4b) reveals a small increase in unsaturation (1600 cm^{-1}) relative to the carbonyl signal at 1740 cm^{-1}, but suggests no major functional change over this temperature range. Despite the observed conservation of carbonyl functionality in the FTIR spectrum of A300, titration reveals a substantial
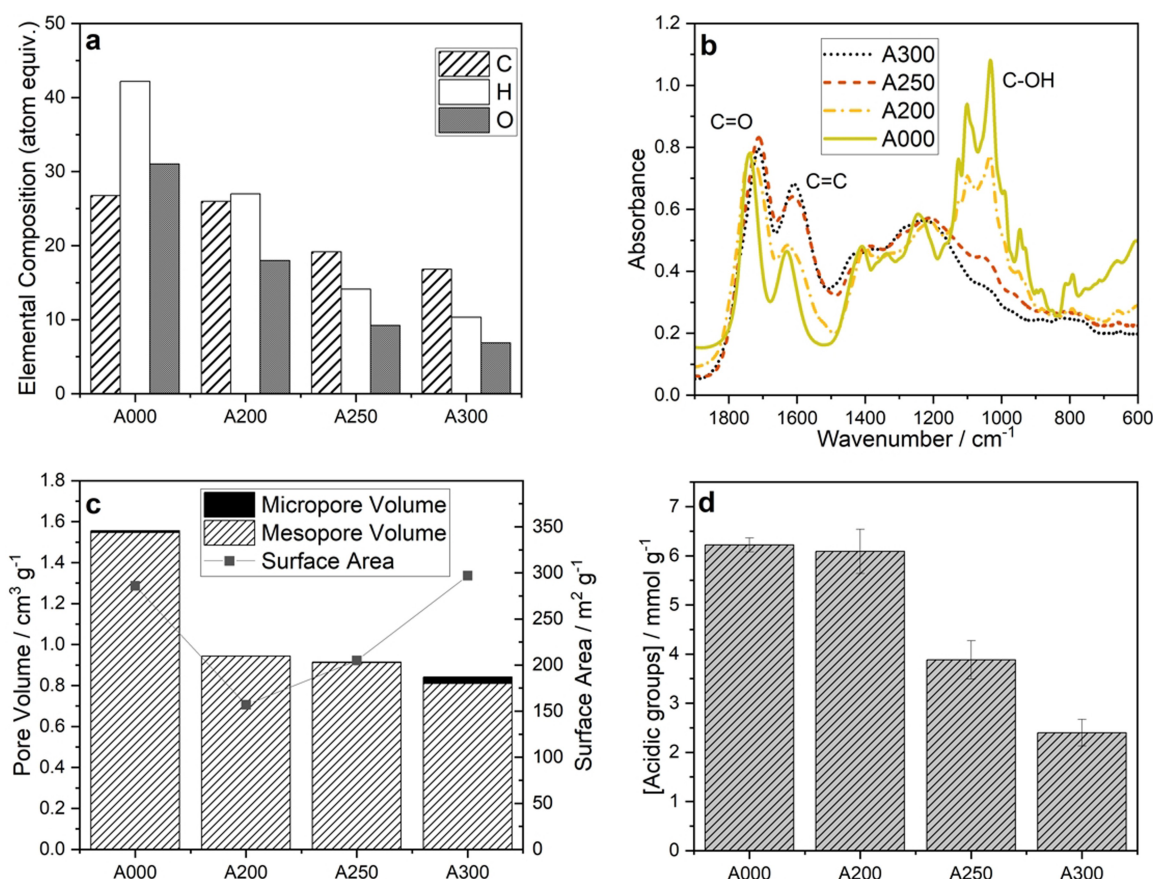
ChemSusChem

Research Article
doi.org/10.1002/cssc.202400015

Chemistry
Europe
European Chemical
Societies Publishing

Figure 4. a) C, H and O elemental composition (atom equiv.) of A000, A200, A250 and A300, scaled according to total mass loss at each pyrolysis temperature. Calculated from thermal analysis and CHN elemental analysis. b) Transmission FTIR spectra of KBr disks containing 0.6 wt% A000 (yellow), A200 (orange), A250 (red) and A300 (black). c) Summary of porous properties of A000, A200, A250 and A300, determined by N2-sorption porosimetry. d) Titration of the total number of acidic groups present in A000, A200, A250 and A300. Error bars used to indicate 95% confidence range.

loss of acidity. This may be rationalised by the growth of a signal at 200 ppm in the ^{13}C NMR spectra that suggests the formation of ketones concurrent with the loss of carboxylate. Between 200 and 300 °C, the apparent increase in micropore volume (0.03 cm^3 g^{-1}) results in a moderate increase in total surface area to 300 m^2 g^{-1} (Figure 4c). It is important to note that the increase in N$_2$ sorption attributed to the formation of micropore may be rationalised in at least two ways, as a result of a genuine change in porous structure and the development of micropore, or as the evolution of volatile organic compounds from pre-existing micropore. While the former is entirely possible, evidence of the latter is seen in the evolution of organic species across this temperature range, as characterised by thermogravimetry-gas chromatography-mass spectrometry (Figure S3).

Cu(II) Adsorption

For more sustainable sorbent materials to be considered for the replacement of incumbent technologies, several aspects of their performance must be evaluated and optimised. While far from the only consideration, a large capacity for metal ions is clearly

an essential component of any sorbent technology and will ultimately determine the mass of sorbent required for a given volume of effluent. To evaluate the metal adsorption capacity of mesoporous alginate-derived materials and to determine the role of pyrolysis temperature, Cu(II) removal from aqueous solutions was determined at pH 4.5 (Figure 5). Adsorption was measured at pH 4.5 to avoid the complication associated with the formation of insoluble copper hydroxides at higher pH. The adsorption capacity of A000 (2.8 mmol g^{-1}) is in very close agreement with that predicted by the theoretical structure of the alginate–M^{2+} chelate (Figure 1) which suggests that Cu(II) is indeed coordinated by two carboxylate groups. A comparison of the copper capacities in Figure 5 reveals the expected loss of metal capacity associated with the decomposition of carboxylate functionality at higher temperatures. Upon pyrolysis to 300 °C, the A000 precursor is seen to lose 75% of its Cu(II) capacity, highlighting the compromise between metal uptake and material stability (discussed below).

To illustrate the influence of porosity on metal uptake and the importance of the Starbon® process in generating the porous A000 precursor, a non-porous A300 equivalent (A300*) was prepared. Pyrolysis of alginic acid without the expansion and freeze-drying steps necessary to introduce porosity,
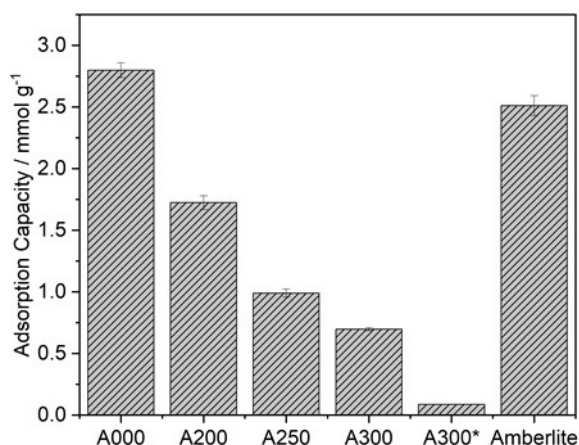
ChemSusChem

Research Article
doi.org/10.1002/cssc.202400015

Chemistry Europe
European Chemical
Societies Publishing

Figure 5. Maximum capacity for Cu(II) at ca. 0.15 g l^{-1} and pH 4.5. A300* is an alginate material pyrolysed without using the Starbon process, resulting in a largely non-porous material. Amberlite™ refers to the commercial weak cation exchanger Amberlite™ Mac-3H. Error bars used to indicate 95% confidence range.

resulted in the effectively non-porous A300* (mesopore volume = 0.04 cm^{3}g^{-1}, surface area = 7 m^{2}g^{-1}) (Table S4). Upon comparison of the capacities of the porous (0.70 mmol g^{-1}) and non-porous (0.09 mmol g^{-1}) materials pyrolysed to 300 °C, it becomes clear that the porous structure accounts for the vast majority of metal uptake. While the external surface area of A300* may facilitate Cu(II) adsorption to a limited extent, the inaccessibility of the majority of carboxylate groups results in poor metal capacity, highlighting the importance of the significant porosity of A300.

Additionally, as an example of a commercially available weak cation exchange resin, the capacity of Amberlite™ Mac-3H was measured. Amberlite™ Mac-3H is a petrochemical-derived macro porous polyacrylate resin functionalised by grafted carboxylate groups and is marketed for the selective adsorption of copper and iron cations from solution. At pH 4.5, the capacity of Amberlite™ Mac-3H (2.51 mmol g^{-1}) was found to be intermediary of A000 and A200, demonstrating the potential for mesoporous alginate-derived materials to be used within similar applications.

Upon adsorption of Cu^{2+} by A000–300, exchange for H$^+$ results in a drop in solution pH. The pH drift recorded in Table 1 corresponds qualitatively to the size of Cu(II) adsorption and confirms that even after pyrolysis, Cu^{2+} is adsorbed via exchange with protons. However, due to the amphoteric nature

of the Starbon® materials, it was not possible to exactly quantify the ratio of H$^+$:Cu^{2+} exchanged. After the initial decrease in pH, each solution was adjusted to pH 4.5 so that adsorption by each material could be compared under identical conditions.

Using the results of titration and Cu(II) adsorption capacities, the relative number of carboxylate groups per Cu^{2+} ion adsorbed (A:Cu) have been calculated (Table 2) Upon pyrolysis to 200 °C, despite the distinct conservation of carboxylate groups, there is substantial change in the stoichiometry of Cu(II) chelation as A:Cu increases from 2.2 to 3.5. This coincides with the major textural changes occurring between 0–200 °C (Figure 4c), caused by dehydration and crosslinking, and appears to result in the change in structure of the metal chelation sites and the increased A:Cu ratio exhibited by A200, A250 and A300. It is suggested that the combination of contracted porous structure and decreased conformational flexibility, due to cross-linking and increased unsaturation, results in decreased accessibility of M^{2+}-coordination sites. Above 200 °C, there is no further change in stoichiometry and so Cu(II) capacity decreases predictably with the decomposition of carboxylate groups.

Adsorption Selectivity

In addition to having large M^{2+} capacities, weak cation exchangers are used because of their ability to selectively remove metals such as Cu and Fe from complex mixtures. As such, it was necessary to evaluate the selectivity of adsorption by A000–300. Selectivity for copper in the presence of nickel and cobalt, was compared for the alginate materials prepared at a range of temperatures and to Amberlite™ Mac-3H.

The relative adsorption of Cu(II), Ni(II) and Co(II) are compared in Figure 6. A000 was found to exhibit very similar selectivity to Amberlite™ Mac-3H, with Cu adsorbed to a much greater extent than both Ni and Co, highlighting the potential for these materials to be used within the same applications for selective Cu adsorption. Selectivity for copper was found to increase slightly at the highest pyrolysis temperatures but generally the same selectivity was exhibited by all the alginate-derived materials. This selectivity may be explained simply in terms of the relative strengths of the M^{2+}-carboxylate complexes formed upon adsorption which is understood to follow the order Cu > Co ≈ Ni, where log(K) values for the formation of 1:1 metal–acetate complexes are found to be 1.76, 0.72 and 0.71 for Cu(II), Ni(II) and Co(II) respectively.[40] The conserved selectivity seen for A200, A250 and A300 provides additional

Table 1. Final pH of solution after Cu(II) adsorption from solution with initial pH 4.

Material	pH after adsorption
A000	2.8
A200	2.9
A250	3.4
A300	3.9

Table 2. Number of carboxylate groups per copper cation adsorbed ([COOH]:Cu^{2+}) for each of the alginate-derived materials studied.

Material	[COOH]: Cu^{2+}
A000	2.2
A200	3.5
A250	3.7
A300	3.4

ChemSusChem

Research Article
doi.org/10.1002/cssc.202400015

Chemistry Europe
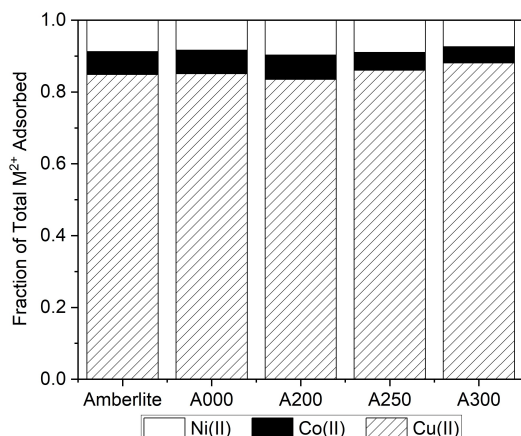European Chemical
Societies Publishing

Figure 6. Selectivity for Cu (stripe), Co (black) and Ni (white) adsorbed from mixed metal solution by amberlite™ and alginate-derived materials. Quantity of metal adsorbed plotted as a fraction of the total metal removed from solution. Starting solution contained Cu, Ni and Co at 3 mmol l^{-1} and at pH 4.5.
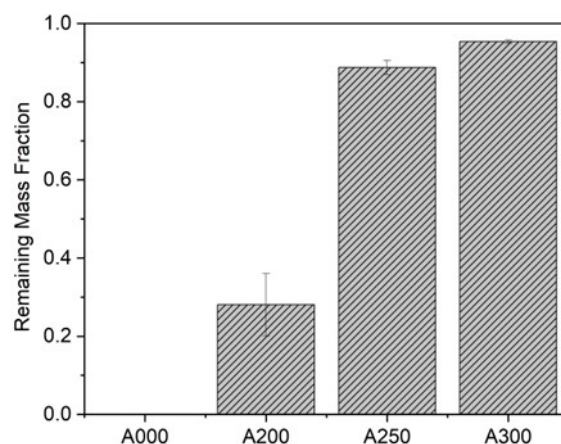

Figure 7. Degree of covalent crosslinking as a function of pyrolysis temperature. Expressed as remaining mass fraction after neutralisation with NaHCO$_3$. Error bars used to indicate 95% confidence range.

evidence that the major interaction responsible for adsorption remains carboxylate complexation.

Degree of Covalent Crosslinking

Arguably the most important aspect of sustainable sorbent design is the ability for the material to be reused indefinitely, as determined by the material's stability. With the excellent capacity and selectivity of alginate-derived materials already known, the primary aim of this work was to determine whether the Starbon® process could be used to impart sufficient chemical stability.

To this end, the degree of covalent crosslinking within the materials produced at a range of temperatures was determined by neutralising each with excess NaHCO$_3$. Neutralising alginic acid using sodium bases is expected to result in the complete conversion to the water-soluble sodium alginate salt. By filtering and weighing the remaining solid, an approximate fraction of the material covalently crosslinked during pyrolysis is obtained (Figure 7).

Despite having the largest capacity for Cu(II), alginic acid is seen in Figure 7 to be entirely solubilised by the presence of Na$^+$ at neutral pH, highlighting the chemical instability of alginate gels. As anticipated, upon pyrolysing A000, the material becomes increasingly covalently crosslinked at higher temperatures. By 200 °C, crosslinking has clearly begun as ~30% of the material mass is seen to remain after neutralisation. The most significant increase in crosslinking occurs between 200 and 250 °C with the material resulting from pyrolysis at 250 °C ~90% crosslinked. This increase in stability is seen to coincide with the later stages of dehydration as monitored using FTIR (Figure 4b). Limited further stability is achieved upon pyrolysis to 300 °C where ~95% of the material remained after neutralisation. As

an approximation for chemical stability, Figure 7 illustrates nicely the temperature range over which crosslinking occurs and the point at which these materials become practically useful in Na-containing solutions.

Conclusions

The global demand for more accessible means to remove heavy metals from industrial effluents and sources of drinking water has prompted a widespread effort to develop more sustainable low-cost sorbent materials. While alginates present a promising abundant and renewable feedstock, the chemical instability of alginate-derived materials precludes their long-term reuse in most cases. By exploring the chemical and structural changes occurring during low temperature pyrolysis, we have evaluated the Starbon® process as a means to impart sufficient chemical stability without entirely compromising the metal chelating properties of alginic acid.

Despite significant changes to the chemical structure of the alginic acid aerogel precursor, materials produced at 200, 250 and 300 °C exhibit substantial M^{2+} capacity and high selectivity for Cu(II) ions in mixed metal systems. Crucial for reusability, intermolecular dehydration between 200–250 °C results in sufficient crosslinking to resist dissolution by Na$^+$ at neutral pH, as is seen for alginic acid.

While this work demonstrates the excellent potential for alginate-derived mesoporous materials to be used in a variety of wastewater remediation applications, further research is necessary. In particular, optimisation of mechanical properties such as particle size and shape, and porous structure would facilitate process development to enable implementation.

As a crisis that disproportionately affects the least developed regions on the planet, technologies that address safe drinking water must, as a priority, be obtained simply and inexpensively from accessible feedstocks.

Experimental Section

Materials

Alginic acid was supplied by Marine Biopolymers. Sodium chloride was purchased from Acros Organics. Copper(II) chloride anhydrous (98%) was purchased from Alfa Aesar. Hydrochloric acid 37% (analytical grade), Sodium bicarbonate and sodium hydroxide were purchased from Fisher. *Tert*-butanol (99%) was purchased from Fluorochem. Spectroscopic grade potassium bromide, nickel chloride hexahydrate (trace metal basis), cobalt chloride (anhydrous) and Amberlite™ Mac-3H Cation Exchange Resin were purchased from Sigma Aldrich.

Alginate Starbon Preparation

A200, A250 and A300 were produced via the freeze-drying method previously described by Borisova et al.[35] Importantly, this methodology enables the recycling and reuse of the *tert*-butanol–water eutectic used in the expansion of the polysaccharide precursor. All materials (A300, A250, A200 and A000) were de-ashed using excess 2 M HCl, equilibrating for 24 hours before washing with excess water until washings were neutral. Starbons have been abbreviated according to existing precedent, by a letter and three numbers where the letter indicates the polysaccharide precursor (starch-S, pectin-P, alginate-A) and the numbers indicate the pyrolysis temperature in degrees Celsius. A000 was gelled and freeze dried under the same conditions as the other materials but was not pyrolysed. After being washed with water the materials were not dried prior to copper adsorption experiments.

A300* was produced by pyrolysing the same alginic acid feedstock (to 300 °C) without the expansion or freeze-drying steps that impart porosity. After pyrolysis, A300* was de-ashed in the same way as all previous materials.

SEM/EDX

Elemental composition of all carbon materials was determined by SEM-EDX (JEOL 7800F Prime SEM). Atom % was averaged over 4 sites per sample. SEM micrographs were obtained at a range of magnifications using the same instrument. Prior to imaging, materials were coated in Pt/Pd to prevent charge build up.

N$_2$-Sorption Porosimetry

The textural properties of A000–300 were determined by N$_2$-sorption porosimetry using a Micromeritics ASAP 2020 volumetric adsorption analyser at 77 K. Prior to analysis, A300, A250 and A200 (~0.15 g) were degassed at 150 °C and 50 μm Hg for 4 hours. To prevent chemical decomposition, and subsequent textural change, A000 was degassed at 75 °C and 50 μm Hg until the mass of the sample remained constant for 5 hours (15 hours total), indicating that the sample had been effectively degassed. Total surface area (S$_{BET}$) was determined using the BET model, mesopore volume (V$_{Meso}$) was estimated using the Barrett-Joyner-Halenda (BJH) desorption method, micropore volume (V$_{Micro}$) was determined using t-plot equation. Materials were analysed prior to de-ashing so that pore structure was not destroyed by the subsequent drying process.

Transmission FTIR

Samples were pressed into KBr disks for analysis by transmission IR. Both spectroscopic grade KBr and analyte were dried under vacuum at 75 °C for at least 3 hours. The sample was diluted in KBr to 0.6 wt% (1.5 mg sample in 250 mg KBr) and ground using agate mortar and pestle before pressing under reduced pressure (50 mbar) at 12 tons of pressure. Spectra obtained were averaged over 4 scans with 1 cm^{-1} resolution on a Perkin Elmer Spectrum Two spectrometer with LiTa detector.

Titration

To determine the total number of acidic surface groups, each material was indirectly titrated with NaOH using a procedure adapted from that proposed by Boehm[9,41] and later developed by Goertzen and Schönherr.[42–44] Ca. 20 mg of material was added to 40 mL of 5 mM NaOH. The slurries were then stirred for 24 hours before filtration through cellulose paper. For each sample, a 5 mL aliquot of base filtrate was added to 10 mL of 5 mM HCl before back titration with NaOH solution. A blank solution of NaOH (with no alginate) was treated in the same way for titration to allow the difference to be calculated as below. Potentiometric titrations were performed on a Metrohm 901 Titrando. The titration endpoint was determined using the first differential of the titration curve. The concentration of surface acid sites C$_{SAS}$ was calculated using Equation 1.

$$C_{SAS} = \frac{\left(V^T_{alg} - V^T_{blank}\right) \times \left[B^T\right] \times V^B}{M_{alg} \times V^A} \tag{1}$$

Where V^T_{alg} and V^T_{blank} are the volumes (mL) of titrant required to neutralise the aliquot of base mixed with alginate material and blank base solutions respectively. $[B^T]$ is the concentration (mmol L^{-1}) of titrant base, in this case 5 mmol NaOH was used. V^B and V^A were the volumes (mL) of base initially added to the alginate sample and the aliquot taken after filtration. M_{alg} is the mass (mg) of alginate sample added to the base.

Thermal Analysis

Thermal analysis was conducted on a Netzsch STA 409 CD Simultaneous Thermal Analyser under flow of nitrogen (100 cm^3 min^{-1}). Ca. 100 mg of A000 was heated to 150 °C at 10 °min^{-1}, followed by heating to 300 °C at 1 °min^{-1}.

CHN Elemental Analysis

CHN analysis was conducted by Exeter Analytical using a CE440 CHN Elemental Analyser. Oxygen content was determined as the remaining wt% after C, H and N were subtracted (on the basis that inorganic content was less than 1% for all materials).

Using thermal analysis mass loss and elemental analysis, the quantity of each element retained from the starting material at each pyrolysis temperature was calculated according to the following:

$$\frac{wt\% \; of \; X \; at \; T_p \times \; wt\% \; of \; sample \; at \; T_p}{100} = proportion \; of \; X \; remaining \tag{2}$$

$$\frac{proportion \; of \; X \; remaining}{atomic \; mass \; of \; X} = equiv. \; of \; X \tag{3}$$

ChemSusChem

Research Article
doi.org/10.1002/cssc.202400015

Chemistry Europe
European Chemical
Societies Publishing

$$\frac{equiv.\ of\ X}{equiv.\ of\ C_{A000}\ +\ equiv.\ of\ H_{A000}\ +\ equiv.\ of\ O_{A000}\ =\ atom\ \%\ of\ A000} \tag{4}$$

Where T_p = pyrolysis temperature of either 0, 200, 250 or 300 °C. X refers to either C, H or O. Wt% of X at T_p determined by CHN analysis. Wt% of sample as determined by thermal analysis at each temperature point.

Copper Adsorption

Maximum adsorption capacity – The copper adsorption capacities of A000, A200, A250, A300, A300* and Amberlite™ Mac-3H were determined using a solution of 0.2 g L^{-1} CuCl$_2$ at pH 4.5. 50–100 mg of alginate material was suspended in 100 mL of CuCl$_2$ solution. After equilibration, initial pH drift was recorded and all solutions were adjusted to pH 4.5 using NaHCO$_3$. Solutions were then equilibrated for 24 hours before filtering using 0.22 μm regenerated cellulose filters and the resulting solution diluted in 4% HNO$_3$ for analysis by Thermo Scientific iCAP 7400 ICP-OES spectrometer. Samples were introduced via auto sampler and intensities were obtained by both axial and radial measurements. pH measurements were made using Jenway 3500 pH Meter fitted with Simple junction universal pH electrode. Adsorption capacity q_e (mg g^{-1}) was determined by Equation 5:

$$q_e = \frac{(C_o - C_e) \times V}{m} \tag{5}$$

Where C_o and C_e are the initial and final metal concentrations (mg L^{-1}), V is the volume (L) of metal solution exposed to the adsorbent and m is the mass (g) of adsorbent.

Adsorption selectivity – The competitive adsorption of Cu, Ni and Co from a mixed metal solution was compared for A000, A200, A250, A300 and Amberlite™ Mac-3H. A solution containing CuCl$_2$, NiCl$_2$ and CoCl$_2$ each at 3 mmol L^{-1} pH 4.5 was used. Based on the previously determined capacities (mmol g^{-1}) of each of the materials and to ensure the same total metal uptake, sorbent was added to 30 mL of solution so that the total concentration of adsorption sites was 3 mmol L^{-1}. After initial equilibration, all solutions were adjusted to pH 4.5 using NaHCO$_3$. Solutions were then equilibrated for 24 hours before filtering using 0.22 μm regenerated cellulose filters and the resulting solution diluted in 4% HNO$_3$ for analysis by ICP-OES as above. To allow comparison of selectivity, the quantity of each metal adsorbed as a fraction of total metal adsorbed was calculated.

Degree of Covalent Crosslinking

To determine the degree of covalent crosslinking in materials produced at a range of pyrolysis temperatures, materials were neutralised with excess NaHCO$_3$. 250 mg (6 mmol g^{-1}) of NaHCO$_3$ was added to approximately 500 mg of A000, A200, A250 or A300 that had been previously washed with HCl and then water. The resulting mixture was stirred for 30 minutes before being centrifuged, filtered and dried. The remaining dry mass as a fraction of the original mass was calculated.

Conflict of Interests

Dr Rob McElroy is CTO of Starbons Ltd, a start-up from the University of York.

Data Availability Statement

The data that support the findings of this study are available from the corresponding author upon reasonable request.

[1] World Health Organization (WHO) and the United Nations Children's Fund (UNICEF), **2021**.
[2] R. S. Boyd, *J. Chem. Ecol.* **2010**, *36*, 46–58.
[3] A. Alengebawy, S. T. Abdelkhalek, S. R. Qureshi, M.-Q. Wang, *Toxics* **2021**, *9*, 42.
[4] P. B. Tchounwou, C. G. Yedjou, A. K. Patlolla, D. J. Sutton, in *Molecular, Clinical and Environmental Toxicology* (Ed.: A. Luch), Springer Basel, Basel, **2012**, pp. 133–164.
[5] S. Bolisetty, M. Peydayesh, R. Mezzenga, *Chem. Soc. Rev.* **2019**, *48*, 463–487.
[6] B. Qiu, X. Tao, H. Wang, W. Li, X. Ding, H. Chu, *J. Anal. Appl. Pyrolysis* **2021**, *155*, 105081.
[7] C. Liu, H.-X. Zhang, *J. Environ. Chem. Eng.* **2022**, *10*, 107393.
[8] Radovic, Ljubisa, Moreno-Castilla, Carlos, Rivera-Utrilla, Jose, in *Chemistry and Physics of Carbon*, Taylor & Francis Group, **2001**, pp. 227–382.
[9] H. P. Boehm, *Carbon* **1994**, *32*, 759–769.
[10] P. Delhaès, Ed., in *Graphite and Precursors*, Gordon and Breach, Amsterdam [u.a], **2001**, pp. 141–179.
[11] X. Yang, Y. Wan, Y. Zheng, F. He, Z. Yu, J. Huang, H. Wang, Y. S. Ok, Y. Jiang, B. Gao, *Chem. Eng. J.* **2019**, *366*, 608–621.
[12] M. Streat, D. J. Malik, B. Saha, in *Ion Exchange and Solvent Extraction*, **2004**, pp. 1–84.
[13] N. A. Chudasama, R. A. Sequeira, K. Moradiya, K. Prasad, *Molecules* **2021**, *26*, 2608.
[14] S. Saji, A. Hebden, P. Goswami, C. Du, *Sustainability* **2022**, *14*, 5181.
[15] E. R. Morris, D. A. Rees, D. Thom, *Carbohydr. Res.* **1980**, *81*, 305–314.
[16] J. S. Craigie, E. R. Morris, D. A. Rees, D. Thom, *Carbohydr. Polym.* **1984**, *4*, 237–252.
[17] T. L. D. Silva, J. M. M. Vidart, M. G. C. D. Silva, M. L. Gimenes, M. G. A. Vieira, in *Biological Activities and Application of Marine Polysaccharides* (Ed.: E. A. Shalaby), InTech, **2017**.
[18] B. Wang, Y. Wan, Y. Zheng, X. Lee, T. Liu, Z. Yu, J. Huang, Y. S. Ok, J. Chen, B. Gao, *Crit. Rev. Environ. Sci. Technol.* **2019**, *49*, 318–356.
[19] X. Guo, Y. Wang, Y. Qin, P. Shen, Q. Peng, *Int. J. Biol. Macromol.* **2020**, *162*, 618–628.
[20] E. L. Hirst, J. K. N. Jones, W. O. Jones, *J. Chem. Soc.* **1939**, 1880–1885.
[21] A. Staby, M.-B. Sand, R. G. Hansen, J. H. Jacobsen, L. A. Andersen, M. Gerstenberg, U. K. Bruus, I. H. Jensen, *J. Chromatogr. A* **2004**, *1034*, 85–97.
[22] S. K. Chanda, E. L. Hirst, E. G. V. Percival, A. G. Ross, *J. Chem. Soc.* **1952**, 1833–1837.
[23] A. Haug, B. Larsen, in *Proceedings of the Fifth International Seaweed Symposium*, Halifax, August 25–28, 1965, Elsevier, **1966**, pp. 71–277.

[24] H. G. Park, T. W. Kim, M. Y. Chae, I.-K. Yoo, *Process Biochem.* **2007**, *42*, 1371–1377.

[25] A. Verma, S. Thakur, G. Mamba, Prateek, R. K. Gupta, P. Thakur, V. K. Thakur, *Int. J. Biol. Macromol.* **2020**, *148*, 1130–1139.

[26] J. Roosen, J. Pype, K. Binnemans, S. Mullens, *Ind. Eng. Chem. Res.* **2015**, *54*, 12836–12846.

[27] L. Zhang, D. Wu, B. Zhu, Y. Yang, L. Wang, *J. Chem. Eng. Data* **2011**, *56*, 2280–2289.

[28] N. M. Mahmoodi, B. Hayati, M. Arami, H. Bahrami, *Desalination* **2011**, *275*, 93–101.

[29] Y. Zhuang, F. Yu, H. Chen, J. Zheng, J. Ma, J. Chen, *J. Mater. Chem. A* **2016**, *4*, 10885–10892.

[30] V. Budarin, J. H. Clark, J. J. E. Hardy, R. Luque, K. Milkowski, S. J. Tavener, A. J. Wilson, *Angew. Chem.* **2006**, *118*, 3866–3870.

[31] V. L. Budarin, P. S. Shuttleworth, R. J. White, J. H. Clark, in *Porous Carbon Materials from Sustainable Precursors* (Ed.: R. J. White), The Royal Society Of Chemistry, **2015**, pp. 53–81.

[32] R. J. White, V. L. Budarin, J. H. Clark, *Chem. Eur. J.* **2010**, *16*, 1326–1335.

[33] A. S. Marriott, A. J. Hunt, E. Bergström, J. Thomas-Oates, J. H. Clark, *J. Anal. Appl. Pyrolysis* **2016**, *121*, 62–66.

[34] M. Inagaki, M. Toyoda, Y. Soneda, S. Tsujimura, T. Morishita, *Carbon* **2016**, *107*, 448–473.

[35] A. Borisova, M. De Bruyn, V. L. Budarin, P. S. Shuttleworth, J. R. Dodson, M. L. Segatto, J. H. Clark, *Macromol. Rapid Commun.* **2015**, *36*, 774–779.

[36] W. Mackie, *Carbohydr. Res.* **1971**, *20*, 413–415.

[37] J. Ayarza, Y. Coello, J. Nakamatsu, *Int. J. Polym. Anal. Charact.* **2017**, *22*, 1–10.

[38] P. S. Shuttleworth, V. Budarin, R. J. White, V. M. Gun'ko, R. Luque, J. H. Clark, *Chem. Eur. J.* **2013**, *19*, 9351–9357.

[39] Y. Liu, Z. Li, J. Wang, P. Zhu, J. Zhao, C. Zhang, Y. Guo, X. Jin, *Polym. Degrad. Stab.* **2015**, *118*, 59–68.

[40] J. W. Bunting, K. M. Thong, *Can. J. Chem.* **1970**, *48*, 1654–1656.

[41] H. P. Boehm, in *Advances in Catalysis*, Elsevier, **1966**, pp. 179–274.

[42] S. L. Goertzen, K. D. Thériault, A. M. Oickle, A. C. Tarasuk, H. A. Andreas, *Carbon* **2010**, *48*, 1252–1261.

[43] A. M. Oickle, S. L. Goertzen, K. R. Hopper, Y. O. Abdalla, H. A. Andreas, *Carbon* **2010**, *48*, 3313–3322.

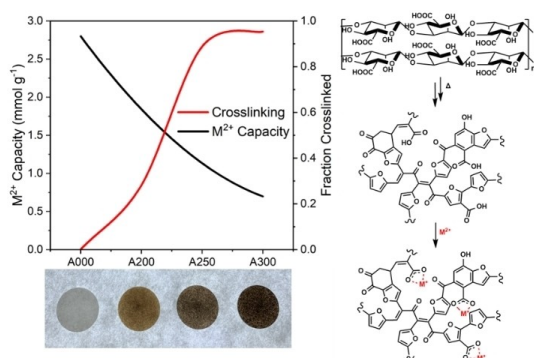[44] J. Schönherr, J. Buchheim, P. Scholz, P. Adelhelm, *C* **2018**, *4*, 21.

RESEARCH ARTICLE

N. Garland*, Dr. R. Gordon, Dr. C. R. McElroy, Prof. A. Parkin, Dr. D. Mac-Quarrie*

1 – 10

Optimising Low Temperature Pyrolysis of Mesoporous Alginate-Derived Starbon® for Selective Heavy Metal Adsorption

Exploring the chemical changes that accompany the low temperature pyrolysis of mesoporous polysaccharide-derived materials (Starbon®) towards the production of sustainable heavy metal adsorbents. Controlled pyrolysis results in extensive covalent crosslinking, imparting chemical stability while maintaining high adsorption capacities (0.70–1.72 mmol g^{-1}) and selectivity for Cu^{2+} over other divalent cations.